Searching for *CP*-even Higgs bosons of the minimal supersymmetric model at hadron supercolliders

John F. Gunion
Department of Physics, University of California, Davis, California 95616

Robert Bork, Howard E. Haber, and Abraham Seiden
Santa Cruz Institute for Particle Physics, University of California, Santa Cruz, California 95064

(Received 9 December 1991)

The branching ratios and supercollider cross sections of the two *CP*-even Higgs scalars h^0 and H^0 of the minimal supersymmetric model (MSSM) are computed (including the effects of leading log radiative corrections). The "gold-plated" Higgs-boson decay into $ZZ \to l^+l^-l^+l^-$ is analyzed at the CERN Large Hadron Collider and Superconducting Super Collider, and the regions of MSSM Higgs sector parameter space where the h^0 or H^0 can be detected in this mode are delineated. The prospects for Higgs-boson detection as a function of the detector resolution are discussed. The viability of other decay modes for detecting the h^0 and H^0 is briefly considered.

PACS number(s): 13.85.Qk, 12.15.Cc, 14.80.Gt

I. INTRODUCTION

A crucial issue for the future of high-energy physics is whether the combination of the CERN e^+e^- collider LEP-200 and the hadron supercolliders CERN Large Hadron Collider (LHC) and the Superconducting Super Collider (SSC) will make it possible to unravel the nature of the Higgs sector [1]. LEP-200 will discover the standard model (SM) Higgs boson if it is lighter than about 90 GeV. The SSC and LHC will be sensitive to heavier Higgs-boson masses, though detection throughout the intermediate-mass region from m_W to $2m_W$ will certainly require the examination of several Higgs-boson production/decay modes and an integrated luminosity of $L=10$ fb^{-1} at the SSC (and considerably more luminosity at the LHC). However, various theoretical arguments suggest that the sector responsible for electroweak symmetry breaking will be more complicated than that of the minimal standard model. Among the theoretical approaches which go beyond the standard model, "low-energy" supersymmetry is particularly attractive and preserves the elementarity of the Higgs bosons. In the minimal supersymmetric extension of the standard model (MSSM), the Higgs sector contains the following physical states: two *CP*-even Higgs scalars (h^0 and H^0 with $m_{h^0} \leq m_{H^0}$), one *CP*-odd Higgs scalar (A^0), and a charged Higgs pair ($H^\pm$). In this paper, we focus on the phenomenology of the neutral *CP*-even scalars.

In the MSSM, all tree-level properties of the Higgs bosons can be computed as a function of m_{A^0}, the mass of the *CP*-odd scalar, and $\tan\beta = v_2/v_1$, where v_2 (v_1) is the vacuum expectation value of the neutral Higgs field which couples to up- (down-)type quarks. For example, given m_{A^0} and $\tan\beta$ we may compute the masses of h^0, H^0, and $H^\pm$ and the angle α which arises in the diagonalization of the *CP*-even Higgs-boson mass matrix. (The angle α appears in various couplings of the Higgs bosons to quarks, vector bosons, etc. [1].) Recently, one-loop radiative corrections to Higgs-boson masses and couplings have been obtained [2–7]. One finds that in addition to m_{A^0} and $\tan\beta$, Higgs-boson masses and couplings also depend on other parameters of the MSSM which enter through virtual loops. In particular, the radiative corrections can be quite large for $m_t \gtrsim 120$ GeV and the corresponding squark masses above (say) 500 GeV. For example, at tree level one finds that $m_{h^0} \leq m_Z$, implying that h^0 could be discovered at LEP-200 (assuming sufficient energy and luminosity). Including radiative corrections, this tree-level bound is *increased* by a term that grows as $m_t^4 \ln(M_{\tilde{t}}^2/m_t^2)$. One finds that $m_{h^0} \lesssim 110$ (140) GeV for $m_t = 150$ (200) GeV and $M_{\tilde{t}} = 1$ TeV. Some of the Higgs-boson couplings are also shifted by significant factors. As a result, for large enough m_t, failure to discover the Higgs boson at LEP-200 will not rule out the MSSM. In this case, it will be crucial to search for the h^0 at the SSC and LHC. Even if the light Higgs boson were discovered at LEP, it would almost certainly possess couplings nearly identical to the Higgs boson of the standard model. Then, in order to distinguish the MSSM Higgs sector from that of the standard model, it would be necessary to search for the other physical Higgs-boson states of the MSSM. Below, we will focus on the search for the H^0.

The search for the H^0 at the SSC and LHC is problematical. The reason for this is connected with the strength of the H^0 coupling to vector-boson pairs, which governs much of the phenomenology of Higgs-boson detection. First, consider the H^0ZZ and $H^0W^+W^-$ tree-level couplings. These are both proportional to $\cos(\beta-\alpha)$, which can be expressed in terms of m_{A^0} and $\tan\beta$. One finds that for large m_{A^0}, this coupling decreases as $m_Z^2/m_{A^0}^2$ and rapidly approaches zero. Over nearly the entire range of parameter space, the coupling of H^0 to W^+W^- and ZZ is significantly suppressed, which severely limits prospects for its discovery at the SSC and LHC. Radiative corrections to the tree-level re-

sults are incorporated in the following way. The complete one-loop leading log radiative corrections to the *CP*-even Higgs-boson mass matrix have been obtained [7]. When this mass matrix is diagonalized, we obtain the radiatively corrected *CP*-even Higgs-boson masses and mixing angle α as a function of m_{A^0}, $\tan\beta$, m_t, and $M_{\rm SUSY}$, which denotes a common scale for supersymmetry-breaking masses, such as $M_{\tilde{t}}$. From this, one obtains the radiatively corrected result for $\cos(\beta-\alpha)$. We exhibit the results of such a calculation in Figs. 1 and 2. Note that the radiatively corrected $\cos(\beta-\alpha)$ still falls rapidly as m_{A^0} increases but is larger than the corresponding tree-level value. This will have the effect of enlarging the region of parameter space in which the H^0 can be detected at the SSC and LHC.

In searching for the H^0 at a hadron supercollider, the cleanest signature is the "gold-plated" decay $H^0\to ZZ\to l^+l^-l^+l^-$ ($H^0\to 4l$ for short). The viability of this signature depends critically on the overall branching ratio into the $4l$ mode. For example, the standard

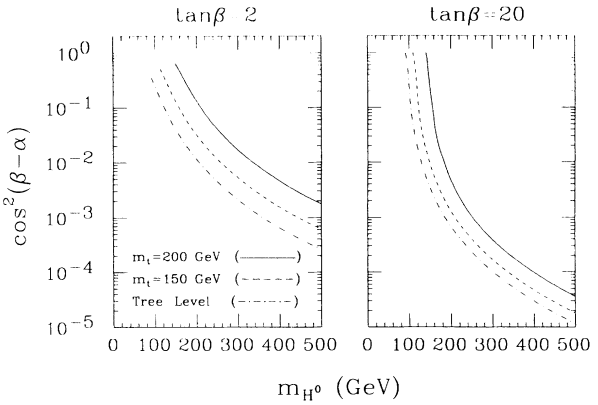

FIG. 2. The value of $\cos^2(\beta-\alpha)$ as a function of m_{H^0} for $\tan\beta=2$ and 20. The tree-level result is shown by the dash-dot curve. The two other curves include the one-loop leading log radiative corrections to $\cos(\beta-\alpha)$ and m_{H^0} (as m_{A^0} is varied) with $m_t=150$ GeV (dashes) and $m_t=200$ GeV (solid), and $M_{\tilde{t}}=1$ TeV (squark mixing has been neglected).

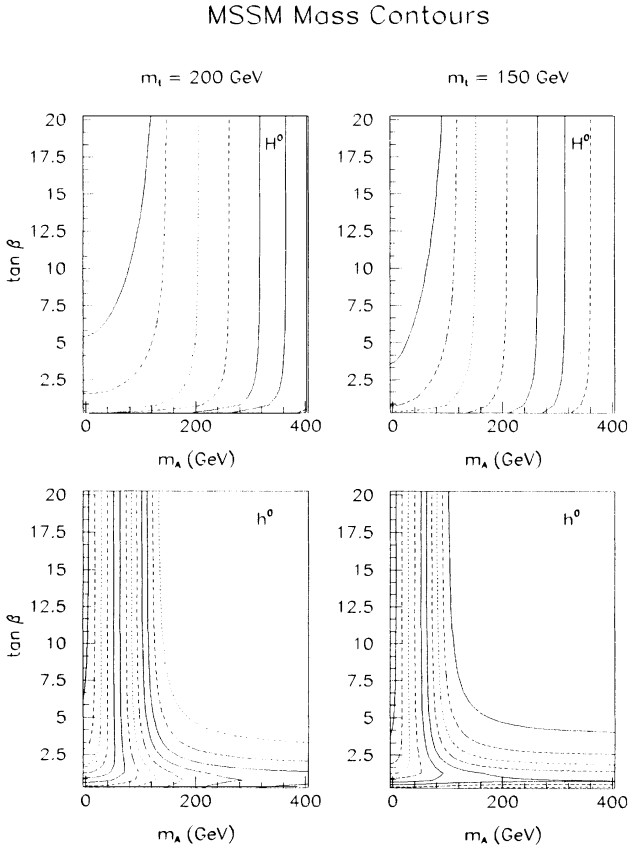

FIG. 1. Mass contours in the m_{A^0}-$\tan\beta$ parameter space for H^0 and h^0 with $m_t=200$ and $m_t=150$ GeV. The H^0 contours begin with 141 GeV (110 GeV) for $m_t=200$ GeV (150 GeV), with the remaining contours being those for $m_{H^0}=150$, 200, 250, 300, and 350 GeV. The h^0 contours run from 10 GeV in steps of 10 GeV to a maximum value of 130 GeV (100 GeV) for $m_t=200$ GeV (150 GeV). These curves include the one-loop leading log radiative corrections with $M_{\tilde{t}}=1$ TeV (squark mixing has been neglected).

model Higgs boson (ϕ^0) can be detected in this mode for $130\lesssim m_{\phi^0}\lesssim 800$ GeV at the SSC with an integrated luminosity of 10 fb^{-1} [1]. Note that for $m_{\phi^0}<2m_Z$, one of the Z bosons is off shell, and the lower limit quoted above corresponds to the point at which the branching ratio into the $4l$ mode is too small. (In contrast, the upper limit quoted above arises from the fact that the production cross section decreases with m_{ϕ^0}.) In the case of the MSSM, the $H^0\to 4l$ decay width is severely suppressed (over a large region of parameter space) in comparison to that of ϕ^0. As a result, the H^0 can be detected at a hadron collider via $H^0\to 4l$ only over a portion of the model parameter space. In this paper, we demonstrate that the region of parameter space allowing such detection at the SSC is surprisingly large, especially if the top-quark mass is large and 30 fb^{-1} of data (i.e., three times the standard SSC yearly integrated luminosity) can be accumulated [8].

There are a number of facts that are responsible for allowing H^0 detection in the $4l$ mode over much of parameter space. First, recall that $\Gamma(H^0\to ZZ)=\Gamma(\phi^0\to ZZ)\cos^2(\beta-\alpha)$ [1]. As a result of the $\cos^2(\beta-\alpha)$ suppression noted above, the $H^0\to ZZ$ decay width is suppressed over nearly all of the model parameter space. Nevertheless, $B(H^0\to ZZ)$ remains close to the corresponding value for the ϕ^0 as long as $\Gamma(H^0\to ZZ)\gtrsim\Gamma(H^0\to Q\bar{Q})$, where Q is the heaviest quark kinematically allowed in H^0 decays. In practice, this is always the case for $m_{H^0}\lesssim 2m_t$ as long as $\tan\beta$ is not very large (thereby enhancing greatly the $H^0\to b\bar{b}$ decays). Second, the generally much smaller values of $\Gamma(H^0\to ZZ, W^+W^-)$ as compared to $\Gamma(\phi^0\to ZZ, W^+W^-)$ (with $m_{\phi^0}=m_{H^0}$) imply that the H^0 is a very narrow resonance below $t\bar{t}$ decay threshold. In fact, for the m_{H^0} values considered in this paper, the total H^0 width is always smaller than the experimental resolution

employed in Sec. III for the $4l$ channel. This has the consequence that in the region $m_{H^0} > 2m_Z$ the $q\bar{q}, gg \to ZZ \to 4l$ background is much smaller than in the ϕ^0 case and is entirely determined by the detector resolution in the $4l$ channel. For our computations in this paper we will consider two possibilities for the $4l$ mass resolution $\Gamma^{\rm res}$ (which is a slowly varying function of M_{ZZ}): a conservative choice based upon early design parameters for the Solenoidal Detector Collaboration (SDC) detector [9] and a more optimistic possibility. Of course, for $m_{H^0} < 2m_Z$ continuum backgrounds to the $4l$ mode are essentially negligible (as in the case of the ϕ^0) provided the resolution in the $4l$ channel is reasonable [10]. In this region, detectability of the H^0 is determined entirely by the absolute event rate.

The main sources for H^0 production are gluon-gluon fusion into H^0 or $H^0 Q\bar{Q}$ (where $Q = t$ or b quark); they provide an ample event sample at the SSC and LHC. The relative importance of these fusion mechanisms depends crucially upon both m_t and $\tan\beta$. The process $gg \to H^0$ is dominant over most of the relevant m_{H^0} range unless $\tan\beta$ is large. For large $\tan\beta$, the $H^0 t\bar{t}$ coupling is suppressed, thereby significantly reducing the size of the (normally) dominant t-quark loop contribution to $gg \to H^0$. The $gg \to H^0 t\bar{t}$ mechanism turns out to vary with $\tan\beta$ much like the $gg \to H^0$ process, but it is always much smaller; nonetheless, for completeness it is included in our cross-section computations. In contrast, the $gg \to H^0 b\bar{b}$ mechanism tends to be dominant for large values of $\tan\beta$ where the $H^0 b\bar{b}$ coupling is enhanced. Indeed, at large $\tan\beta$ the production cross section for the H^0 can be even larger than that for a ϕ^0 of similar mass. On the other hand, an enhanced $H^0 b\bar{b}$ coupling at large $\tan\beta$ implies an enhanced value for $\Gamma(H^0 \to b\bar{b})$ which results in a further suppression of $B(H^0 \to 4l)$. For large enough $\tan\beta$ at a given value of m_{A^0}, this latter suppression is the dominant effect, and H^0 detection in the $4l$ mode may become impossible.

Radiative corrections to the MSSM Higgs sector can have a significant impact on the phenomenology of h^0. In particular, if the h^0 is somewhat heavier than the Z it will not be observable at LEP-200. In Fig. 3 we plot contours in m_{A^0}-$\tan\beta$ parameter space corresponding to several choices for the number of events obtained after including a detection efficiency of 25%. Values of $m_t = 200$ and 150 GeV are considered with $M_{\tilde{t}} = 1$ TeV; squark mixing is neglected.[1] If one adopts the criterion that 25 observed events are needed for discovery, then there are substantial portions of parameter space for which discovery of the h^0 is not possible using either $h^0 Z$- or $h^0 A^0$-associated production. For large m_t the region for which LEP-200 will discover the h^0 is quite restricted. Turning to the SSC and LHC, the detectability of $h^0 \to 4l$ is determined almost entirely by whether m_{h^0} is sufficiently above m_Z so that the $h^0 \to ZZ^* \to 4l$ decay has an adequate branching ratio. (The production cross section for the h^0 from the various gluon-gluon fusion processes noted previously is generally quite substantial.) Of course, the h^0 will be a narrow resonance.

In Sec. II, we survey the branching ratios of H^0 and h^0 (including the leading log radiative corrections) and their primary production cross sections. In Sec. III, we examine the gold-plated $4l$ detection mode for the H^0 and h^0 and determine the range of MSSM parameter space for which detection is possible. Brief remarks concerning detection of the $H^{\pm}$ and other channels for detection of

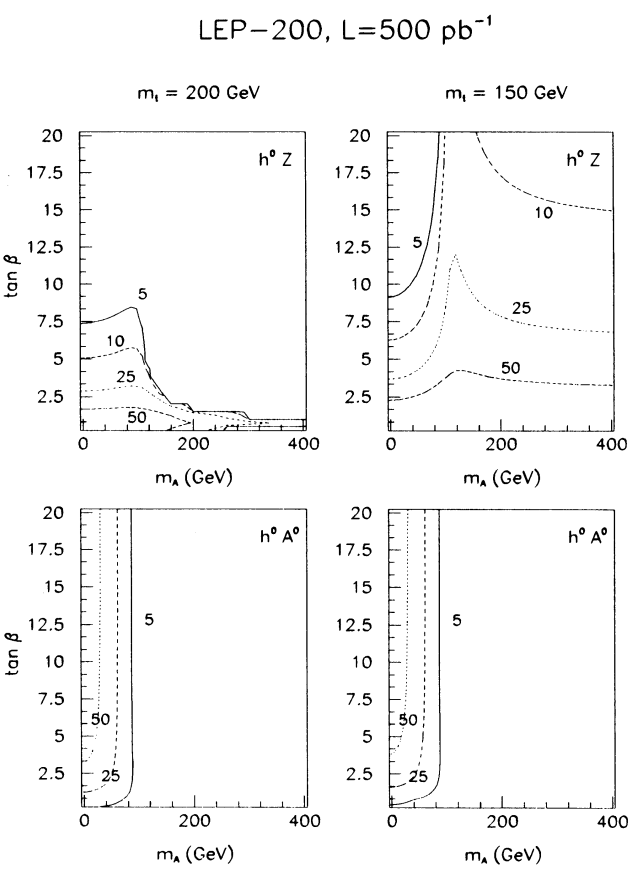

FIG. 3. Event number contours in m_{A^0}-$\tan\beta$ parameter space for $e^+e^- \to h^0 Z$ and $e^+e^- \to h^0 A^0$ at LEP-200 with $\sqrt{s} = 200$ GeV and an integrated luminosity of $L = 500$ fb^{-1}. Results are presented for the two top-quark mass values of $m_t = 150$ and $m_t = 200$ GeV. We have taken $M_{\tilde{t}} = 1$ TeV and have neglected squark mixing. We have included an average detection efficiency factor of 25%. The event number for each contour shown is given on the figure. Assuming that discovery is possible if at least 25 events remain after including the detection efficiency, there is a substantial region where neither process is viable.

[1]The results of Fig. 3 have been obtained using the complete leading log radiative corrections to the MSSM Higgs-boson masses and couplings given in Ref. [7]. It is interesting to note that the parameter-space regions outlined in Fig. 3 are quite sensitive to the precise form of these corrections. For example, if one only includes the leading m_t^4 corrections, the region of parameter space where h^0 detection at LEP-200 is possible would shrink.

the H^0 and h^0 are given in Sec. IV. Final conclusions are presented in Sec. V. Complementary work concerning the search for Higgs bosons of the MSSM at the SSC and LHC appears in Ref. [11].

II. BRANCHING RATIOS AND CROSS SECTIONS FOR THE *CP*-EVEN HIGGS SCALARS

In this section, we will present the two key ingredients for assessing the detectability of the *CP*-even Higgs bosons of the MSSM: namely, their branching ratios to a variety of channels and their production cross sections.

A. Branching ratios

In this section, we collect results for the branching ratios of the h^0 and H^0 of the MSSM. The relative branching ratios of the various channels will determine the feasibility of numerous possible Higgs-boson signatures at the SSC and LHC. The basic tree-level formulas for the various decay rates can be found in Ref. [1]. Here, we improve on these results by incorporating the complete leading log one-loop radiative corrections in the calculation. First, we compute the leading log radiative corrections to the running quartic Higgs-boson self-couplings. We impose supersymmetric boundary conditions at $\mu=M_{\rm SUSY}$, the scale which characterizes the typical size of supersymmetry-breaking masses (e.g., squark and gaugino masses). At $\mu=M_{\rm SUSY}$, these couplings are related to gauge couplings. We then use renormalization-group equations to run the Higgs-boson self-couplings and gauge couplings down to $\mu=m_t$. Finally, we decouple the top-quark and run the couplings down to m_Z. We can then express the physical-Higgs-boson masses and self-couplings in terms of the Higgs-boson self-couplings evaluated at m_Z. We diagonalize the radiatively corrected *CP*-even Higgs-boson mass matrix to obtain the mixing angle α, which appears in the couplings of the Higgs boson to the quarks, leptons, and gauge bosons. Details of this procedure and the relevant formulas can be found in Ref. [7].

We compute the h^0 and H^0 branching ratios as a function of m_{h^0} and m_{H^0}, respectively, by varying m_{A^0} (starting from $m_{A^0}=0$), for various choices of $\tan\beta$ and m_t. The scale of supersymmetry breaking (e.g., the common squark mass) is taken to be $M_{\rm SUSY}=1$ TeV, and $\tilde{t}_L$-$\tilde{t}_R$ mixing is neglected. It is expected that $1 \lesssim \tan\beta \lesssim m_t/m_b$, so we have chosen two representative values: $\tan\beta=2$ and 20. We will present results for $m_t=150$ and 200 GeV. Supersymmetric particles are assumed to be sufficiently massive so that associated two-body decay channels are kinematically forbidden and loops involving such particles contribute negligibly to one-loop-induced couplings. Finally, we note that the QCD correction to Higgs-boson decay to $b\bar{b}$ has been included. This effect is roughly a 50% reduction from the non-QCD-corrected width, and is mostly attributable to the running of the b-quark mass from $2m_b$ to the Higgs-boson mass. Our results for the h^0 are shown in Figs. 4 and 5 and those for the H^0 in Figs. 6 and 7. Below ZZ (WW) threshold, the curves labeled ZZ (WW) correspond to the case in which one of the Z (W) bosons is virtual.

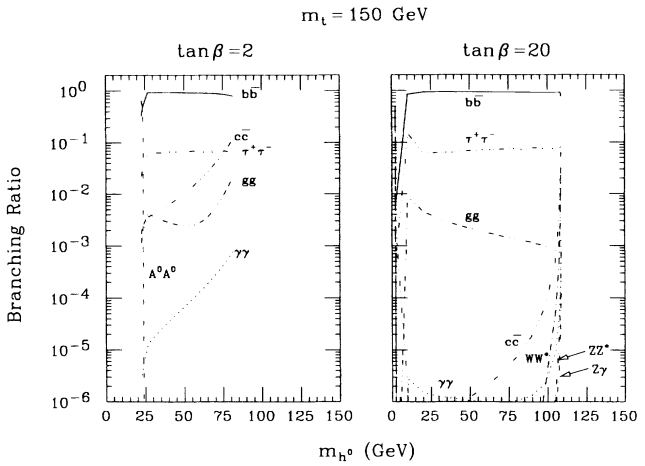

FIG. 4. Branching ratios for the h^0 computed for $m_t=150$ GeV and for $\tan\beta=2$ and 20. One-loop radiative corrections have been included as described in the text. The notation for the curves follows: $b\bar{b}$ (——); W^+W^- (—·—·—·); ZZ (··—··—); A^0A^0 (·—··—); $c\bar{c}$ (···—); $\tau^+\tau^-$ (····—); $\gamma\gamma$ (·····); $Z\gamma$ (··——); gg (···———).

We briefly note a number of important features of these results. First, in the case of the h^0 we find that there is a tiny region near the lower limit of m_{h^0} for which $h^0 \to A^0A^0$ decay is kinematically possible, and in that region it is completely dominant. Once m_{A^0} becomes large enough that this decay is forbidden, the $b\bar{b}$ mode is always dominant, followed by the $\tau^+\tau^-$ mode. Typically, gg and $c\bar{c}$ are the next largest modes (but significantly below $\tau^+\tau^-$). When m_{h^0} approaches its upper limit, ZZ^* and WW^* modes can be significant. In this region the one-loop-induced decays $\gamma\gamma$ and $Z\gamma$ have branching ratios of order 10^{-3}. However, we note that

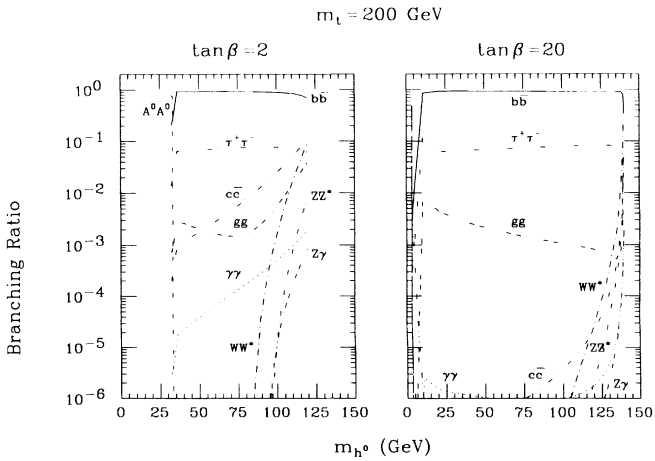

FIG. 5. Branching ratios for the h^0 computed for $m_t=200$ GeV and for $\tan\beta=2$ and 20. One-loop radiative corrections have been included as described in the text. The notation for the curves is that specified in the caption for Fig. 4.

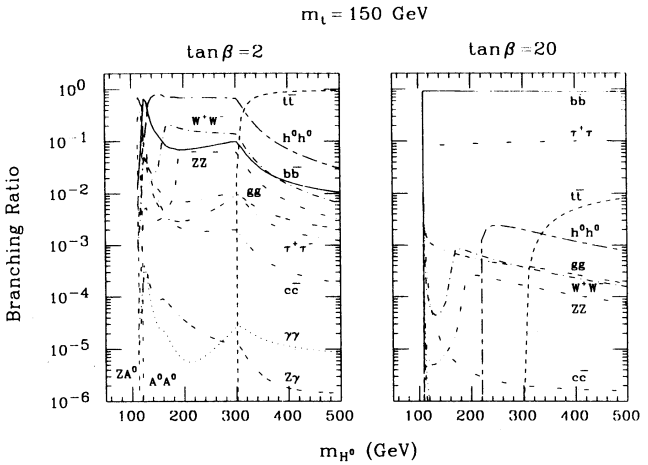

FIG. 6. Branching ratios for the H^0 computed for $m_t = 150$ GeV and for $\tan\beta = 2$ and 20. One-loop radiative corrections have been included as described in the text. The notation for the curves follows: $b\bar{b}$ (——); $t\bar{t}$(— — — —); W^+W^- (—·—·—·); ZZ (··—··—); ZA^0 (·——·——); A^0A^0 (·—··—); h^0h^0 (—·—·); $c\bar{c}$ (···—); $\tau^+\tau^-$ (·····—); $\gamma\gamma$ (·····); $Z\gamma$ (··— —); gg (··· — —).

m_{h^0} must be very near to its maximum allowed value in order that its couplings approach those for a standard model ϕ^0 of the same mass. In this case, all the branching ratios approach those of the ϕ^0 at the corresponding mass.

Turning to the H^0, we observe a plethora of channels, especially at the smaller value of $\tan\beta$. For the very smallest allowed m_{H^0} values (corresponding to small m_{A^0} values), the two most important modes are $H^0 \to h^0h^0$ and $H^0 \to A^0A^0$, where the former is completely dominant for $\tan\beta = 2$, but the latter becomes competitive at $\tan\beta = 20$. At $\tan\beta = 2$, the $H^0 \to h^0h^0$ mode typically continues to dominate until m_{H^0} passes the $t\bar{t}$ threshold,

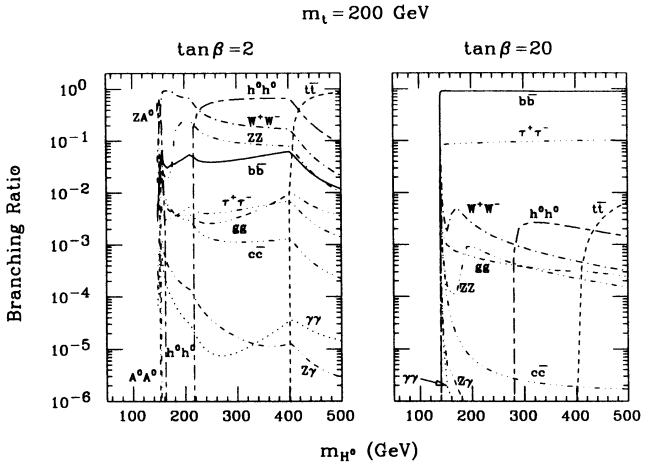

FIG. 7. Branching ratios for the H^0 computed for $m_t = 200$ GeV and for $\tan\beta = 2$ and 20. One-loop radiative corrections have been included as described in the text. The notation for the curves is that specified in the caption for Fig. 6.

except for a region of moderate m_{H^0} where it is kinematically suppressed or forbidden. At $\tan\beta = 2$, we also see that WW and ZZ decays remain important below $t\bar{t}$ threshold (as noted earlier), and $b\bar{b}$ decays are almost never above 20%. For $\tan\beta = 2$, the $t\bar{t}$ channel is dominant when not kinematically suppressed or forbidden. At $\tan\beta = 20$, the systematics are quite different. Once m_{H^0} is above the very small range near its lower bound where h^0h^0 and A^0A^0 modes combine to dominate the H^0 decays, $b\bar{b}$ decays take over, even above $t\bar{t}$ threshold. Moreover, (at $\tan\beta = 20$) the $\tau^+\tau^-$ branching ratio is typically of order 10%, whereas ZZ and WW channels never exceed 1%.

In Sec. III we will primarily make use of the branching ratios to ZZ. In Sec. IV we will comment on some of the implications of the other decay modes for MSSM Higgs-boson searches at the SSC and LHC.

B. Cross sections

In computing production cross sections for h^0 and H^0 we have included three processes: $gg \to h^0(H^0)$, $gg \to h^0(H^0) + b\bar{b}$, and $gg \to h^0(H^0) + t\bar{t}$. The latter is never very important for inclusive h^0, H^0 production, but is presented here since it plays an important role in searches for the h^0 and H^0 in the $l\gamma\gamma$ final-state mode that will be briefly discussed in Sec. IV and is analyzed in detail in Ref. [12]. The WW fusion cross sections are always substantially smaller than the total cross section from other subprocesses. In the case of the h^0, the WW fusion cross section is not significant simply because m_{h^0} is relatively small, and either the $gg \to h^0$ or $gg \to h^0 + b\bar{b}$ cross section is generally much larger. In the case of the H^0, WW fusion is negligible over much of parameter space since the H^0WW coupling is generally strongly suppressed, as illustrated in Fig. 2. The H^0WW coupling is only a significant fraction of standard model strength if m_{H^0} is not very far above its lower limit and $\tan\beta$ is large. In this latter region of parameter space, m_{H^0} is sufficiently low so that the $gg \to H^0 + b\bar{b}$ cross section is much larger than the $WW \to H^0$ cross section. The $W^* \to Wh^0$ process yields an even smaller cross section as compared to the processes already discussed, and will not be presented. It does, however, play a role in h^0 detection in the above-mentioned $l\gamma\gamma$ mode. The $W^* \to WH^0$ cross section is generally very small due to the suppression of the H^0WW coupling constant.

Returning to the primary production processes, we would like to make note of a few calculational details. The $gg \to$ Higgs boson $+ b\bar{b}$ cross section has been computed in the $b\bar{b}$ fusion approximation, valid in the limit[2]

[2]In fact, the $b\bar{b}$ fusion approximation overestimates the cross section somewhat, particularly in the Higgs-boson mass range below 500 GeV (e.g., see Ref. [13]). We have also not included the effects of higher-order QCD corrections, which enhance the cross section and are often summarized by a K factor larger than 1.

of $m_{\text{Higgs}} \gg 2m_b$. In this calculation, $\sigma(b\bar{b} \rightarrow \text{Higgs boson})$ is proportional to the width $\Gamma(\text{Higgs boson} \rightarrow b\bar{b})$, which we have computed including the QCD corrections of Ref. [1] (see also Ref. [14]). The effect of these QCD corrections is to reduce $\sigma(b\bar{b} \rightarrow \text{Higgs boson})$ by about a factor of 2 due to the decrease of the running b-quark mass for $m_{\text{Higgs}} \gg 2m_b$. For the $gg \rightarrow \text{Higgs boson} + t\bar{t}$ cross section we employ the exact tree-level result (without QCD corrections), which has been computed in Ref. [15].

Cross sections for the primary Higgs-boson production processes are displayed in Figs. 8–10. From the plots of h^0 production, we see that for m_{h^0} very near its upper limit all cross sections approach the corresponding cross section for a standard model Higgs boson of the same mass. More generally, as m_{H^0} (and m_{A^0}) becomes large, all the h^0 couplings approach those of the standard model Higgs boson [e.g., in this limit $\sin(\beta-\alpha) \rightarrow 1$, as can be seen from Fig. 2]. Coupled with the growing significance of the ZZ^* decay mode when m_{h^0} approaches its upper limit (as noted in Sec. II A), we conclude that only in this latter parameter regime can the $h^0 \rightarrow 4l$ decay signature be significant. Turning to the H^0, we see that for $\tan\beta < 1$, the $gg \rightarrow H^0$ fusion mechanism is dominant and exceeds that obtained for a standard model Higgs boson of the same mass. At $\tan\beta = 1$, the H^0 and standard model Higgs-boson gg fusion cross sections are relatively similar, but for large $\tan\beta$ the $gg \rightarrow H^0$ cross section is substantially suppressed below the standard model $gg \rightarrow \phi^0$ result. However, we also observe that when $\tan\beta$ is large the $gg \rightarrow H^0 b\bar{b}$ cross section becomes greatly enhanced, and can even exceed $\sigma(gg \rightarrow \phi^0)$ for a standard model Higgs boson of the same mass. Thus, if h^0 or H^0 (or both) lie in the intermediate Higgs-boson mass region, the raw number of Higgs-boson events per year at the LHC and SSC is substantial. Of course, whether these Higgs-boson events are observable depends critically on the specific signature and the corresponding backgrounds.

III. THE GOLD-PLATED FOUR-LEPTON DISCOVERY CHANNEL

A. The H^0 and h^0 signals

In this section we present our computations for the number of $4l$ events resulting from H^0 and h^0 production and decay at the SSC and LHC, including one-loop radiative corrections to the MSSM Higgs sector. The main

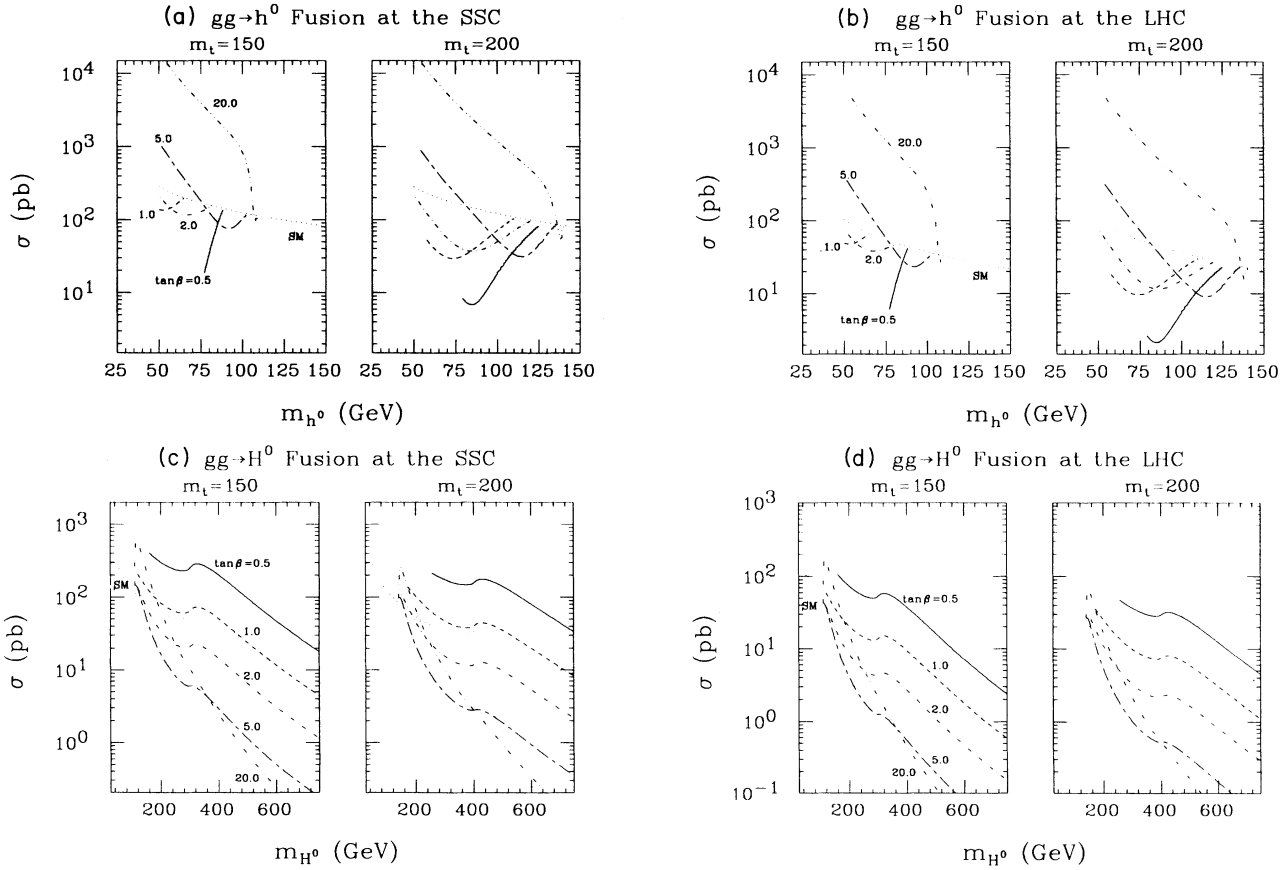

FIG. 8. The cross sections for $gg \rightarrow$ Higgs boson as a function of the Higgs-boson mass. Results are presented for $m_t = 150$ and $m_t = 200$ GeV and for $\tan\beta$ values of 0.5 (——); 1.0 (— — — —); 2.0 (—·—·—·); 5.0 (—··—··); and 20.0 (···—···—). The different cases are (a) h^0 production at $\sqrt{s} = 40$ TeV; (b) h^0 production at $\sqrt{s} = 16$ TeV; (c) H^0 production at $\sqrt{s} = 40$ TeV; (d) H^0 production at $\sqrt{s} = 16$ TeV. Also shown in each case is the corresponding cross section for the standard model (SM) Higgs boson (·····).

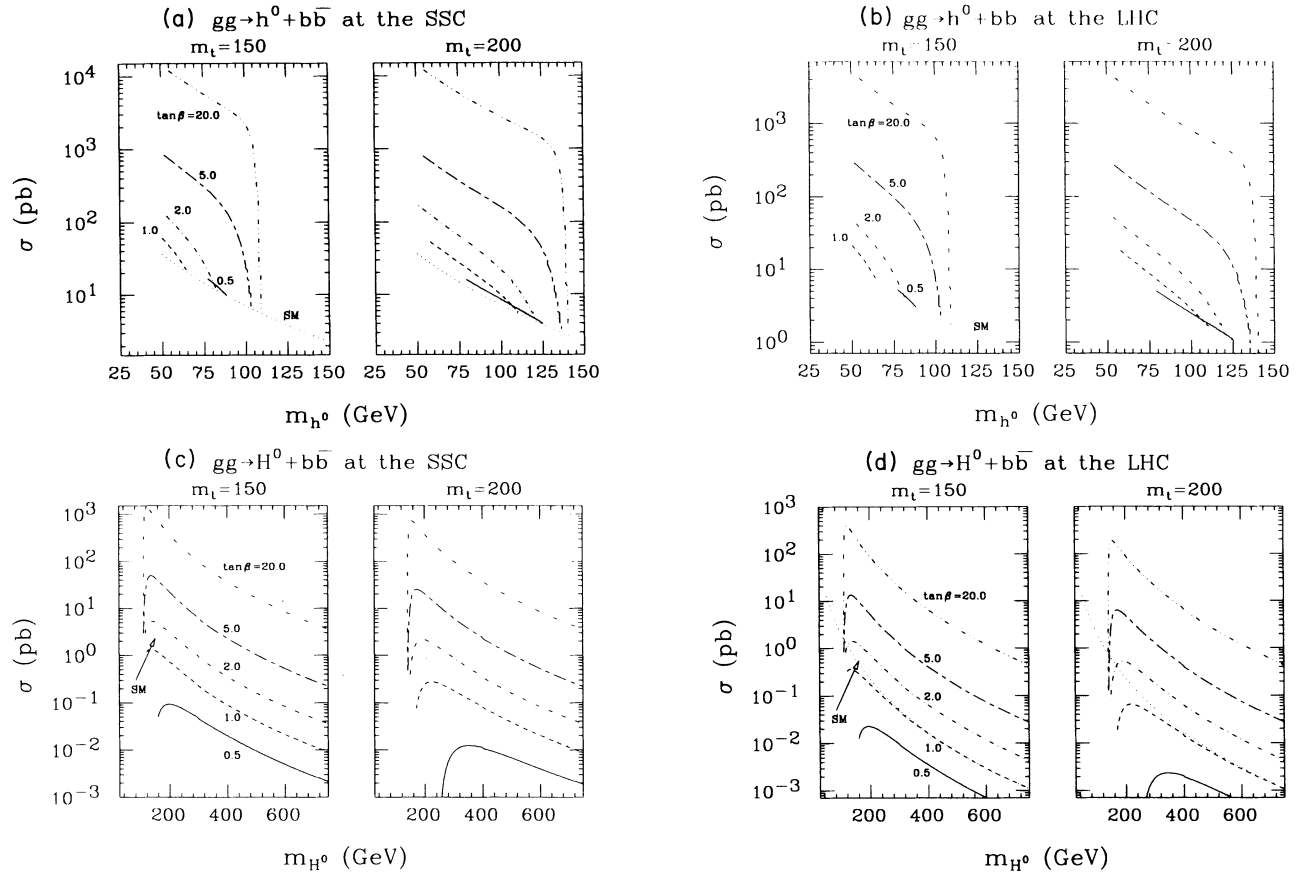

FIG. 9. The cross sections for $gg \rightarrow$ Higgs boson $+b\bar{b}$ as a function of Higgs-boson mass. The different cases and curve notation are as described for Fig. 8.

effect of the radiative corrections compared to tree-level predictions is to modify the values for $m_{h^0}, m_{H^0}, m_{H^\pm}$, and α (α is the mixing angle obtained upon diagonalizing the CP-even sector) found for given input values of m_{A^0} and $\tan\beta$. Corrections to the trilinear Higgs-boson self-couplings can also be important but play only a small role here. In the previous section we have evaluated the partial decay rates of the H^0 and h^0 into its most important channels.

In our computations, we again consider $m_t = 150$ and $m_t = 200$ GeV and adopt supersymmetric parameters as specified in Sec. II. As is evident from Figs. 4–7, the minimum values of m_{h^0} and m_{H^0}, as well as the maximum value of m_{h^0}, depend significantly upon both m_t and $\tan\beta$, even when all other parameters are fixed.

In computing production cross sections for the H^0 we have included three processes: $gg \rightarrow H^0$, $gg \rightarrow b\bar{b}H^0$, and $gg \rightarrow t\bar{t}H^0$, as described in Sec. II B. The latter is always much smaller than $gg \rightarrow H^0$, but it is included for completeness. We have employed the Harriman-Martin-Roberts-Stirling set-B [HMRS(B)] [16] distribution functions ($\Lambda_{\overline{\rm MS}} = 0.19$ GeV, where $\overline{\rm MS}$ denotes the modified minimal subtraction scheme) and have obtained raw cross sections and event rates before any cuts. We have computed event rates at both the LHC and SSC for an integrated luminosity of $L = 30$ fb^{-1} after summing over $l = e, \mu$ channels. This choice of L is made on the basis that it is a reasonable expectation for three years running at the SSC. We have estimated the effects of realistic detector cuts and efficiencies using results quoted in the SDC letter of intent (LOI) [9] as follows.

(1) For the first lepton from each Z we have included a detection efficiency (for a lepton in the detector coverage region) of 0.85. For the second lepton from each Z the SDC LOI indicates that the detection requirements can be relaxed, leading to a detection efficiency of 0.95.

(2) To eliminate random backgrounds, isolation is required for each lepton. The SDC LOI quotes an efficiency of 0.95/lepton for their isolation procedure.

(3) Finally, we must include the efficiency for finding all four charged leptons inside the detector coverage of $|y| < 2.5$, denoted ϵ_y.

The net efficiency factor is then

$$\epsilon = (0.95 \times 0.85)^2 \times (0.95)^4 \times \epsilon_y = 0.531 \times \epsilon_y \ , \qquad (1)$$

where we have adopted the approximate value of $\epsilon_y = 0.70$, independent of Higgs-boson mass. This estimate is based upon SDC studies performed in Ref. [17] and agrees with our Monte Carlo results. Thus, the raw

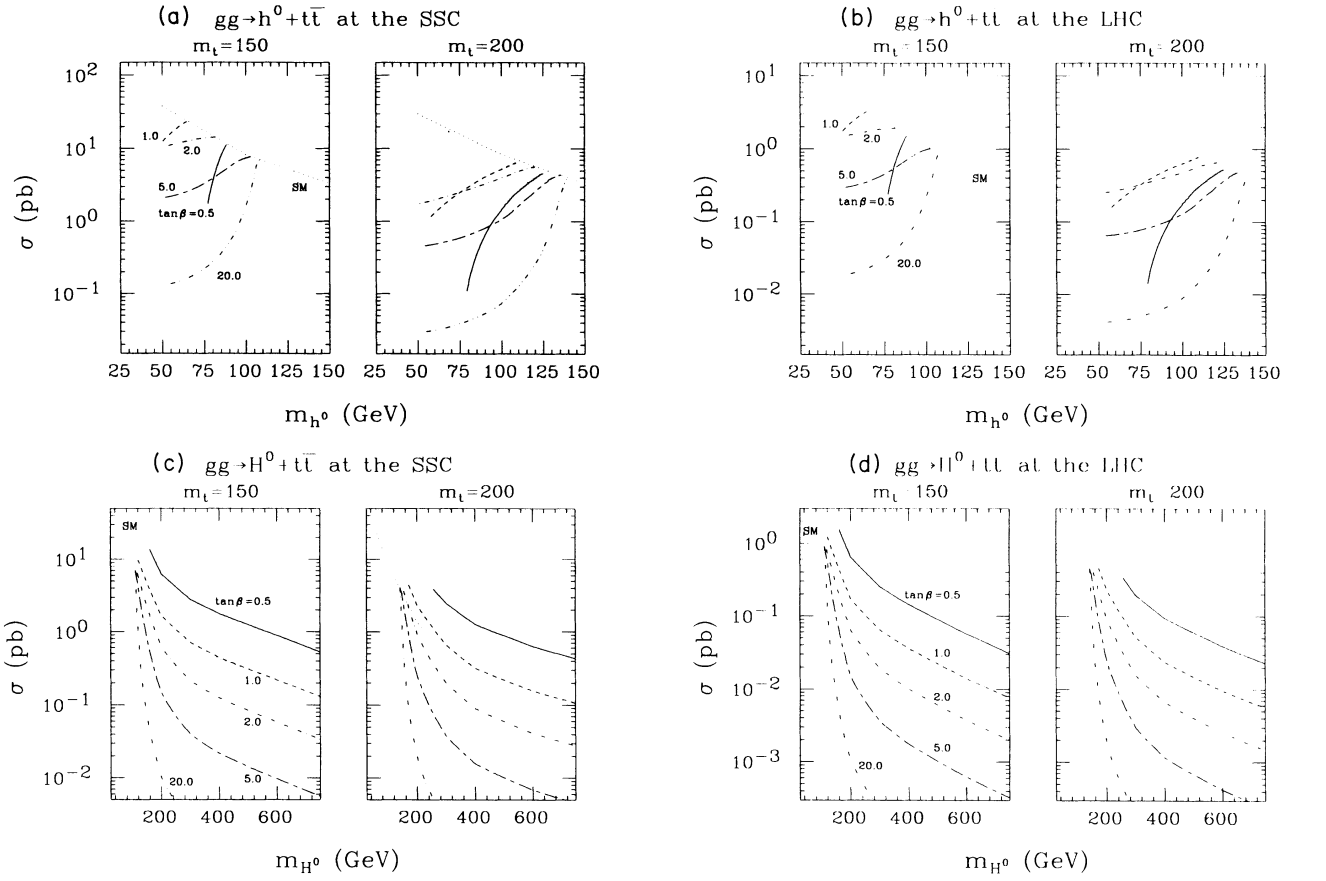

FIG. 10. The cross sections for $gg \rightarrow$ Higgs boson $+t\bar{t}$ as a function of Higgs-boson mass. The different cases and curve notation are as described for Fig. 8.

signal rates will be multiplied by a factor of roughly 0.35 in computing realistic detector event rates.

Finally, as previously noted, for H^0 masses below $2m_Z$, the signal event rate can still be substantial by virtue of the $H^0 \rightarrow ZZ^* \rightarrow 4l$ decays, in which one of the Z's is off shell. This possibility is included in our computations.

B. The ZZ continuum background

The only background that we shall explicitly include is $q\bar{q}, gg \rightarrow ZZ \rightarrow 4l$. Other backgrounds are much smaller once the isolation and other cuts delineated in the SDC LOI are imposed. In computing the number of background events at the SSC we employ the results of Figs. 17 and 18 of the SDC LOI, which include all the above mentioned efficiencies as well as the requirement that there be two lepton pairs, each with $m_{ll}=m_Z \pm 10$ GeV. We have checked these background rates[3] using a Monte Carlo calculation (and multiplying by experimental efficiencies). Scaling to the lower LHC energy has been performed using the results of the latter Monte Carlo program and the same experimental efficiencies. In addition, it is necessary to know what resolution in the $4l$-invariant mass is possible. We shall give results for two extreme assumptions. First, we consider the conservative values obtained in the SDC LOI of $\Gamma^{\rm res}=4.8$ GeV at $m_{4l}=200$ GeV and $\Gamma^{\rm res}=14.0$ GeV at $m_{4l}=400$ GeV. ($\Gamma^{\rm res}$ for other invariant masses is obtained by linear interpolation or extrapolation.) We shall also give results for technically feasible, but certainly optimistic, choices of $\Gamma^{\rm res}=2.2$ GeV at $m_{4l}=200$ GeV and $\Gamma^{\rm res}=5.1$ GeV at $m_{4l}=400$ GeV. The conservative and optimistic possibilities for $\Gamma^{\rm res}$ are labeled below by I and II, respectively. In computing the signal versus background rates, we shall integrate over a bin size of $2\Gamma^{\rm res}$ in order to include essentially 100% of the signal events coming from the (very narrow) Higgs-boson resonance. For $4l$ masses below $2m_Z$, we do not compute the irreducible $4l$ background from the ZZ continuum. As noted earlier, studies [10] have shown that it is essentially negligible by virtue of the fact that one of the Z's must be produced off shell. In addition, cuts can be implemented that are highly efficient for the signal but virtually eliminate other Zl^+l^- backgrounds.

[3]The continuum ZZ background employed by the SDC analysis does not include one-loop QCD corrections. However, the QCD corrections are less than 30% for ZZ-invariant masses less than 400 GeV [18] and do not alter our conclusions.

C. Results

Our results for the H^0 are summarized in a series of figures. First, we consider results obtained for the SSC. In Figs. 11 and 12 we display the $4l$ event rates (including the efficiency factor of $\epsilon=0.35$) from H^0 production and decay at the SSC with $L=30$ fb^{-1} for $m_t=150$ and 200 GeV, respectively. Results for various values of tanβ are illustrated. Also displayed for masses above $2m_Z$ is the minimum event number as a function of mass that is required to obtain a 4σ statistical significance, assuming the conservative and optimistic $4l$ mass resolutions $\Gamma_{\rm I}^{\rm res}$ and $\Gamma_{\rm II}^{\rm res}$. As mentioned earlier, the background is essentially negligible below $2m_Z$. We adopt the criterion that 15 observed events would constitute an identifiable signal. From these two figures, it is evident that for tan$\beta\lesssim 3$ the H^0 can generally be detected via its $4l$ decays in the entire region $2m_Z\lesssim m_{H^0}\lesssim 2m_t$. Further, event rates are often adequate for a substantial region both below and above this range as well, especially for the small and moderate tanβ values. For $m_t=150$ GeV, as tanβ increases beyond 3, one rapidly loses sensitivity to the H^0 except in the region of $m_{H^0}\sim 200$ GeV, and by tan$\beta=20$ detection of the $H^0\to 4l$ decays becomes impossible for all values of m_{H^0}. In contrast, for $m_t=200$ GeV the region of $m_{H^0}\lesssim 2m_Z$ retains adequate event rate (at least 15 events, but more typically two or three times this number) all the way up to tan$\beta=20$.

Of course, these figures can easily be adjusted for different possible values of the accumulated luminosity L. If only $L=10$ fb^{-1} is available, then detection limits for $H^0\to 4l$ can be read off by looking for the points at which the signal and minimum 4σ event rate curves cross *after* decreasing the signal event rate curves by a factor of $\sqrt{3}$ (equivalent to decreasing the signal curves by a factor of 3 and the minimal 4σ event rate curves by a factor of $\sqrt{3}$). By performing this exercise, one easily sees that, with only $L=10$ fb^{-1}, detection of $H^0\to 4l$ would be difficult for tan$\beta\sim 3$ in some of the mass region $m_{H^0}\lesssim 2m_t$. Nonetheless, for m_{H^0} near (but below) $2m_t$, the H^0 would still be observable.

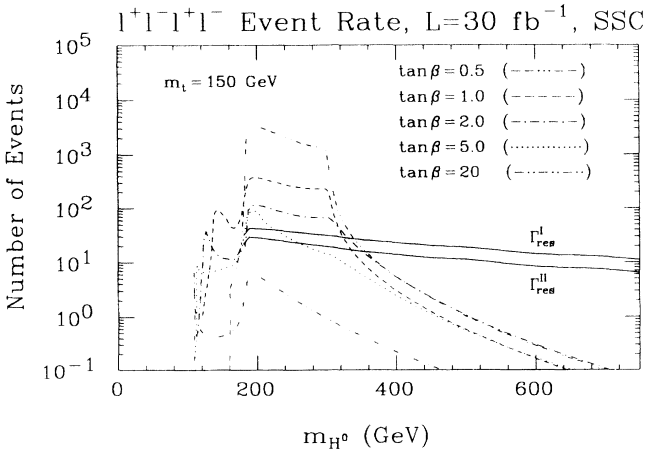

FIG. 11. $4l$ event rates for $L=30$ fb^{-1}, $\epsilon=0.35$, and $m_t=150$ GeV at the SSC compared to the minimum number required for a 4σ effect. The $H^0\to 4l$ signal curves are tan$\beta=0.5$ ($\cdots-$); tan$\beta=1$ ($-\,-\,-\,-$); tan$\beta=2$ ($-\cdot-\cdot-$); tan$\beta=5$ ($\cdots\cdots$); and tan$\beta=20$ ($\cdots-\cdots-$). The two 4σ curves (——) correspond to $\Gamma_{\rm I}^{\rm res}$ and $\Gamma_{\rm II}^{\rm res}$ (see text). Other supersymmetric-model parameters are specified in the text.

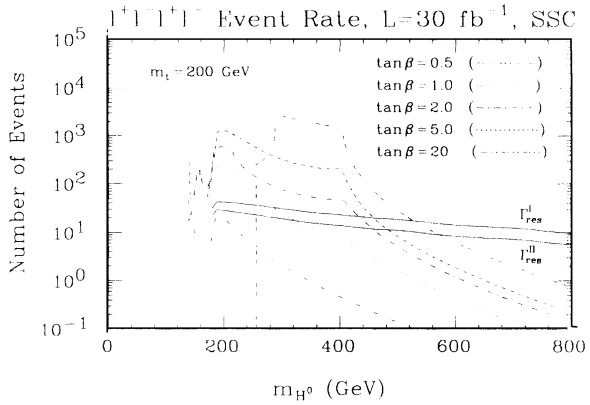

FIG. 12. $4l$ event rates for $L=30$ fb^{-1}, $\epsilon=0.35$, and $m_t=200$ GeV at the SSC compared to the minimum number required for a 4σ effect. Notation as in Fig. 11.

Using the results of Figs. 11 and 12 we can determine the region of m_{A^0}-tanβ parameter space corresponding to a detectable signal for $H^0\to 4l$. For $m_{H^0}>2m_Z$, we plot in Fig. 13 contours corresponding to various fixed values for the ratio $S/\sqrt{B}$, where S is the $H^0\to 4l$ event rate and B is the background event rate as described in Sec. III B.[4] As indicated in Figs. 11 and 12 (and as discussed above), we choose $S/\sqrt{B}=4$ as our criterion for discovery. For $m_{H^0}<2m_Z$, there is essentially no background, and our criterion for discovery corresponds to 15 signal events. In this mass region, the labels on a contour are given by $\frac{4}{15}$ times the number of signal events. In this way contours labeled by the number 4 always correspond to our discovery limit. All event rates include the efficiency reduction factor of $\epsilon=0.35$. We give results for $m_t=150$ and 200 GeV, assuming $L=30$ fb^{-1} at the SSC and the choice of $\Gamma_{\rm I}^{\rm res}$. We see from Fig. 13 that a search for $H^0\to 4l$ decays at the SSC will probe a large region of the overall parameter space of the Higgs sector of the MSSM, provided significant integrated luminosity is obtained. Clearly a large value for m_t would be an advantage in that much more of parameter space could be probed.

Turning now to the h^0, we do not present explicit event rates as a function of m_{h^0} since the results are easily summarized. For $m_t=150$ GeV, even for large tanβ and m_{A^0}, the h^0 is never heavy enough for the $h^0\to ZZ^*\to 4l$

[4]We choose to examine $S/\sqrt{B}$ rather than $S/\sqrt{S+B}$ since it is probable that B will be well determined from the background measured away from the Higgs-boson resonance peak region.

detection mode to have an adequate event rate (15 events after including efficiencies) to allow its detection.[5] In contrast, for $m_t = 200$ GeV, and for all tanβ values considered, m_{h^0} always eventually becomes substantially larger than m_Z as m_{A^0} is taken large. Further, for large enough m_{A^0} the h^0 couplings become standard model like. Thus, one obtains in excess of 15 events over a very substantial region of the m_{A^0}-tanβ parameter space plane. Contours for the h^0 appear in Fig. 13. As above, since $m_{h^0} < 2m_Z$, the labels on a contour are given by $\frac{4}{15}$ times the number of signal events, so that the number 4 always corresponds to our discovery limit. From these contours, we see that detection of $h^0 \to 4l$ at the SSC for $m_t = 150$ is simply not possible. Even if $L = 100$ fb^{-1} of integrated luminosity is accumulated there is no region of parameter space for which one obtains more than three h^0 events after including the $\epsilon = 0.35$ detection efficiency. In contrast, at $m_t = 200$ GeV, the $H^0 \to 4l$ and $h^0 \to 4l$ discovery regions combine to guarantee that at least one or the other will be found at the SSC (for $L = 30$ fb^{-1}) for any m_{A^0}-tanβ parameter combination, and for some choices of these parameters detection of both the h^0 and H^0 will be possible.

At the LHC, event rates for $H^0 \to 4l$ and $h^0 \to 4l$ are typically smaller by a factor of between 4 and 5.5, depending upon the Higgs-boson mass. Meanwhile, the $ZZ \to 4l$ continuum background (to the H^0 decays for

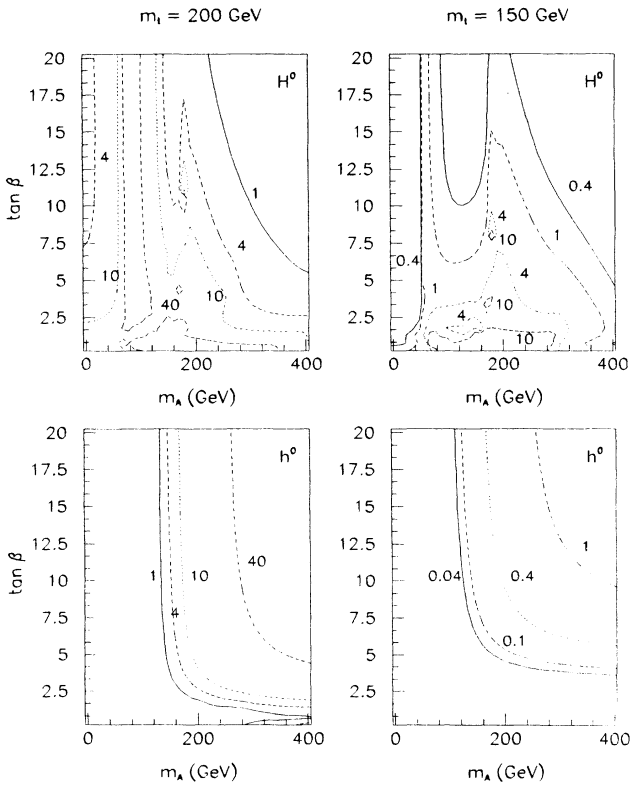

FIG. 13. Contours in tanβ-m_{A^0} parameter space for the SSC with $L = 30$ fb^{-1}. For Higgs-boson mass above $2m_Z$, the numbers on the contours label $S/\sqrt{B}$ as described in the text. Conservative $4l$ mass resolution $\Gamma_l^{\rm res}$ is adopted, and experimental detection efficiency of $\epsilon = 0.35$ is assumed. Our discovery criterion corresponds to the $S/\sqrt{B} = 4$ contour lines. Values employed for the various supersymmetric-model parameters are as specified in the text. Results for other integrated luminosities can be determined by noting that $S/\sqrt{B}$ scales according to $\sqrt{L/30}$ (L in fb^{-1}). For Higgs-boson mass below $2m_Z$, the labels on a contour are given by $\frac{4}{15}$ times the number of signal events. In this way contours labeled by the number 4 always correspond to our discovery limit.

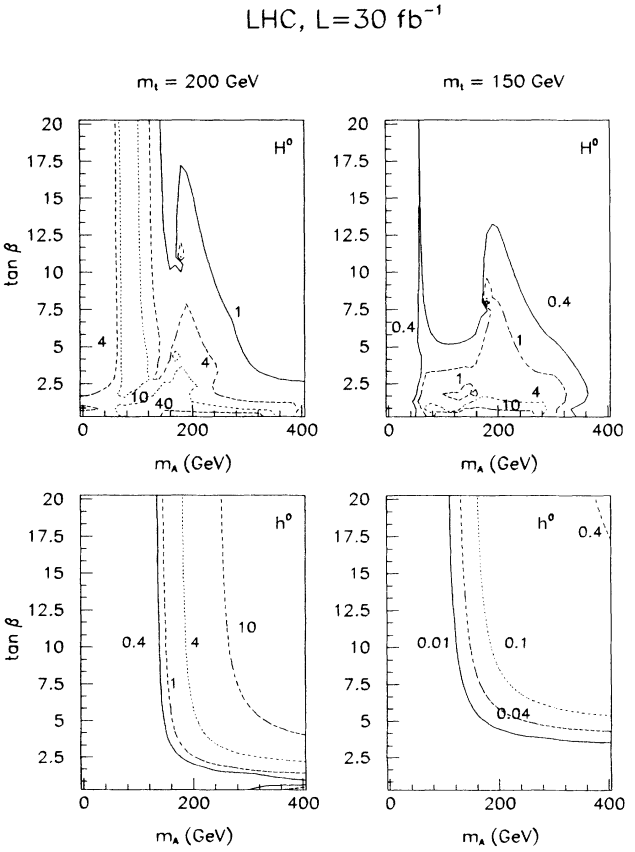

FIG. 14. Contours in tanβ-m_{A^0} parameter space for the LHC ($\sqrt{s} = 16$ TeV) with $L = 30$ fb^{-1}. Our discovery criterion corresponds to the contours labeled by the number 4. See the caption to Fig. 13 for further details.

[5]We note that this conclusion is very sensitive to the exact value predicted for the upper limit of the h^0 mass at large tanβ and m_{A^0}. We have used only leading log formulas for the radiative corrections, which will differ from the exact one-loop result by a few GeV. For example, at $m_t = 150$, if h^0 were 5 GeV heavier than given by our results then $h^0 \to 4l$ decays would be detectable over a large segment of the corner of parameter space where both m_{A^0} and tanβ are large. Of course, this area of parameter space would quickly close if m_t (and therefore m_{h^0}) were slightly reduced in value.

$m_{H^0} > 2m_Z$) decreases only by roughly a factor of 2, implying a factor of $\sqrt{2}$ decrease in the 4σ event-level criterion. (For H^0 or h^0 mass below $2m_Z$ we continue to require at least 15 events.) Therefore, the regions of the parameter space over which the H^0 and h^0 can be detected at the LHC are significantly smaller than those which can be covered by the SSC for the same $L=30$ fb^{-1} integrated luminosity. These regions are shown in Fig. 14. One observes that even for $m_t=200$ GeV there are two sections of the m_{A^0}-tanβ parameter space where neither the H^0 nor the h^0 can be detected at the LHC. These two sections are given approximately by $m_{A^0} \lesssim 60$ GeV, tan$\beta \gtrsim 2.5$ and $120 \lesssim m_{A^0} \lesssim 180$ GeV, tan$\beta \gtrsim 3$–4, respectively. As previously illustrated in Fig. 3, the region of small m_{A^0} with tanβ above about 3 is one in which h^0 (and A^0) detection at LEP-200 will be possible for $L=500$ pb^{-1} in the $e^+e^- \to Z^* \to h^0 A^0$ process. But the region of moderate $m_{A^0} \sim 150$ GeV with tanβ above 3–4 is one for which none of the neutral MSSM Higgs bosons will be detected at LEP-200 (for $m_t=200$ GeV).

Of course, the $4l$ mode is not the only means by which the SSC and LHC might be sensitive to the MSSM Higgs sector in the above particular regions of parameter space. We now turn to a brief summary of other possible scenarios for detection of the MSSM Higgs bosons.

IV. OTHER CHANNELS FOR HIGGS DETECTION

As remarked earlier, the $4l$ mode is not the only one that can be considered for detection of the *CP*-even neutral Higgs bosons of the MSSM. A particularly important possibility is detection of either the h^0 or H^0 in the two-photon decay mode. This is explored in Ref. [12], where it is shown that $t\bar{t}h^0$ associated production, followed by $t \to Wb \to l\nu b$ decay and $h^0 \to \gamma\gamma$ decay, is detectable throughout much of parameter space, even for the relatively modest $M_{\gamma\gamma}$ resolution of the SDC detector [9]. In contrast, it is shown in both Refs. [12] and [19] that, due to the large $q\bar{q}, gg \to \gamma\gamma$ continuum background, detection of inclusive h^0 production followed by decay to $\gamma\gamma$ requires $M_{\gamma\gamma}$ resolution that is significantly better than the planned resolution for the SDC detector. In particular, a resolution in $M_{\gamma\gamma}$ of order 1–2 GeV is required in order for the inclusive $h^0 \to \gamma\gamma$ mode to be viable over a significant region of parameter space.[6] Turning to the heavier *CP*-even scalar, there is only a very narrow region of parameter space in which $H^0 \to \gamma\gamma$ can be detected in the processes described above.

The h^0 can also be produced as a decay product of heavier states. For example, in the case of moderate tanβ the decay mode $A^0 \to Zh^0$ has a very large branching ratio for $m_{A^0} < 2m_t$ (see, for instance, Refs. [1,20]). If efficient tagging of the b quarks from $h^0 \to b\bar{b}$ decay is possible, then the A^0 and h^0 could be detected in the $l^+l^-b\bar{b}$ final state.

Other channels that deserve exploration are apparent from the branching ratio curves (Figs. 4–7). Perhaps most notable among these is the $\tau^+\tau^-$ decay mode, which is generally quite significant ($\sim 10\%$) for both the h^0 and H^0. Detection of the *CP*-even neutral Higgs bosons in this channel when the Higgs-boson mass is in the vicinity of m_Z will almost certainly be very difficult due to the large $Z \to \tau^+\tau^-$ background. Therefore, $h^0 \to \tau^+\tau^-$ detection is not likely to be viable. If m_{H^0} is sufficiently above m_Z and the production cross section is large enough (which requires tan$\beta \gtrsim 10$ in order that the $b\bar{b}$ fusion cross section is greatly enhanced), detection of the $\tau^+\tau^-$ decay mode may turn out to be feasible both in the $e+\mu$ and the $e,\mu+\tau$-jet final states. Some initial investigation of the viability of the related $A^0 \to \tau^+\tau^-$ detection channel can be found in Ref. [11].

At moderate tanβ, the $t\bar{t}$ decay mode of the H^0 is dominant if kinematically allowed, and one can consider the detection of $t\bar{t}H^0$ associated production, followed by $H^0 \to t\bar{t}$. The $t\bar{t}t\bar{t}$ ($4t$) continuum QCD background cross section is of similar size to the $4t$ rate obtained from the Higgs-boson signal [21]. Consequently, if one could efficiently trigger on the $4t$ final state in such a way as to eliminate the many (much larger) reducible backgrounds, isolation of an H^0 signal in this channel might be possible. In the case where $2m_{h^0} < m_{H^0} < 2m_t$ and tanβ is not too large, $H^0 \to h^0h^0$ is the dominant H^0 decay mode. Then, $t\bar{t}H^0 \to W^+W^-b\bar{b}b\bar{b}b\bar{b}$ could provide a viable signature, especially if m_{h^0} is already known. Highly efficient b tagging would be required in order to trigger on the W^+W^-6b final state in order to discriminate against backgrounds.

Evaluation of the viability of all of the above modes requires detailed Monte Carlo simulations, including detector effects and a realistic assessment of QCD backgrounds. However, we are optimistic that the signatures discussed above will provide at least weak signals for the *CP*-even Higgs bosons in the regions of parameter space that we have outlined.

Although not the main topic of this paper, it is of interest to note that for large m_t the region over which $t \to H^+b$ decays can be detected in $t\bar{t}$ production events is non-negligible. Indeed, so long as this decay is not kinematically suppressed or forbidden, studies [22] suggest that it will be easily detected because of the large number of top quarks produced. In fact, Ref. [23] asserts that $t \to H^+b$ decays will be detectable in the tan$\beta \gtrsim 0.5$ region so long as $B(t \to H^+b) \gtrsim 0.003$. This is yet another example in which the detectability of the MSSM Higgs bosons improves as m_t becomes larger. Indeed, for $m_t=200$ GeV one will be able to observe at least one (or in some regions, two or more) of the relatively clean Higgs-boson production-detection modes $H^0 \to 4l, h^0 \to 4l, t\bar{t}h^0 \to l\gamma\gamma$, or $t \to H^+b$ throughout essentially all of m_{A^0}-tanβ parameter space, at both the SSC and the LHC.

[6] It is not excluded that another SSC detector and one or more of the LHC detectors could have the required resolution.

V. CONCLUSIONS

Our most important conclusion is that the SSC with $L=30$ fb^{-1} is capable of detecting $H^0\to 4l$ decays so long as $2m_Z \lesssim m_{H^0} \lesssim 2m_t$ and $\tan\beta \lesssim 3$. Sensitivity to masses and $\tan\beta$ values outside these ranges is also non-negligible, and, in fact, is quite substantial for $m_t=200$ GeV when $m_{H^0}<2m_t$. The region of the m_{A^0}-$\tan\beta$ parameter space in which this decay can be detected is illustrated in Fig. 13. We have also noted that if $m_t=200$ GeV, the radiative correction to the h^0 mass is sufficiently large (when $M_{\tilde{t}}\sim 1$ TeV) that $h^0\to 4l$ decays are detectable over a large region of parameter space (also illustrated in Fig. 13). Of course, it is important to remember that we have assumed that the neutralinos and charginos of the MSSM are sufficiently heavy that the Higgs bosons possess no supersymmetric decay modes. If allowed, such channels would tend to dominate the Higgs-boson decays, and new detection methods would have to be devised.

In our analysis, we have adopted detector efficiencies and resolutions that are typical of the SDC detector as proposed in the SDC LOI. We have shown that technically feasible improved resolution in the $4l$-invariant mass would be helpful in extending the range of m_{H^0} that can be covered at a given $\tan\beta$, but it would not provide a dramatic increase. Event rate is far more critical, and if only $L=10$ fb^{-1} of accumulated luminosity were obtained, or if the detector rapidity coverages (assumed to be $|y|<2.5$ in our analysis) were decreased, our ability to detect the H^0 in the $4l$ mode would generally be marginal for m_{H^0} values near $2m_t$ when $\tan\beta \gtrsim 4$, and some of the accessibility of the h^0 in the case where $m_t=200$ GeV would be eliminated.

At $m_t=200$ GeV the discovery regions for the H^0 and h^0 combine so that at least one of the two *CP*-even Higgs bosons of the MSSM will be discovered for any choice of m_{A^0} and $\tan\beta$. This is not the case at $m_t=150$ GeV. Indeed, for $m_t \lesssim 150$ GeV an important goal will be to determine if the $H^0\to 4l$ search considered here can be combined with searches for other MSSM Higgs-boson decays, many of which were outlined in Sec. IV, so as to guarantee that the SSC is capable of discovering one or more of the MSSM Higgs bosons. Alternatively, by considering a suitable combination of modes, one could hope to demonstrate that if none are found at the SSC then the MSSM would be ruled out.

ACKNOWLEDGMENTS

This project benefited from the U.C. Davis Workshop on Higgs/EWSB Physics at Hadron Supercolliders. Two of us (J.F.G. and H.E.H.) are grateful for the hospitality of the Aspen Center for Physics where part of this work was completed. This work was supported in part by the Department of Energy.

[1] J. F. Gunion, H. E. Haber, G. Kane, and S. Dawson, *The Higgs Hunter's Guide* (Addison-Wesley, Redwood City, CA, 1990).

[2] H. E. Haber and R. Hempfling, Phys. Rev. Lett. **66**, 1815 (1991).

[3] J. Ellis, G. Ridolfi, and F. Zwirner, Phys. Lett. B **257**, 83 (1991); **262**, 477 (1991); A. Brignole, J. Ellis, G. Ridolfi, and F. Zwirner, *ibid.*, **271**, 123 (1991).

[4] Y. Okada, M. Yamagushi, and T. Yanagida, Prog. Theor. Phys. **85**, 1 (1991); Phys. Lett. B **262**, 54 (1991).

[5] R. Barbieri and M. Frigeni, Phys. Lett. B **258**, 395 (1991).

[6] A. Yamada, Phys. Lett. B **263**, 395 (1991).

[7] H. E. Haber, in Proceedings of the International Workshop on Electroweak Symmetry Breaking, Hiroshima, Japan, 1991 (unpublished); H. E. Haber and R. Hempfling, Santa Cruz Institute for Particle Physics Report No. SCIPP-91/33, 1992 (unpublished).

[8] This conclusion was already apparent from the tree-level investigation that appears in J. F. Gunion, in Proceedings of the WHEPP-II Workshop, Calcutta, India, 1991 (unpublished).

[9] SDC Collaboration, Letter of Intent, Publication No. SDC-90-00151, 1990.

[10] J. F. Gunion, G. L. Kane, and J. Wudka, Nucl. Phys. **B299**, 231 (1988). For a recent experimental treatment, see Ref. [9].

[11] Z. Kunszt and F. Zwirner, in *Proceedings of the ECFA Large Hadron Collider Workshop*, Aachen, Germany, 1990, edited by G. Jarlskog and D. Rein (CERN Report No. 90-10, Geneva, Switzerland, 1990), Vol. II, p. 578; Report No. ETH-TH/91-7, 1991 (unpublished); V. Barger, M. S. Berger, A. L. Stange, and R. J. N. Phillips, Phys. Rev. D **45**, 4128 (1992).

[12] J. F. Gunion and L. Orr, this issue, Phys. Rev. D **46**, 2052 (1992).

[13] D. A. Dicus and S. Willenbrock, Phys. Rev. D **39**, 751 (1989).

[14] M. Drees and K. Hikasa, Phys. Lett. B **240**, 455 (1990); **262**, 497(E) (1991).

[15] Z. Kunszt, Nucl. Phys. **B247**, 399 (1984).

[16] P. N. Harriman, A. D. Martin, W. J. Stirling, and R. G. Roberts, Phys. Rev. D **42**, 798 (1990).

[17] J. Hylen *et al.*, Santa Cruz Institute for Particle Physics Report No. SCIPP-90-24, 1990 (unpublished).

[18] B. Mele, P. Nason, and G. Ridolfi, Nucl. Phys. **B357**, 409 (1991); J. Ohnemus and J. F. Owens, Phys. Rev. D **43**, 3626 (1991).

[19] H. Baer, M. Bisset, C. Kao, and X. Tata, Phys. Rev. D **46**, 1067 (1992).

[20] J. F. Gunion, H. E. Haber, and C. Kao, Phys. Rev. D (to be published).

[21] Z. Kunszt, Nucl. Phys. **B247**, 399 (1984); V. Barger, A. Stange, and R. J. N. Phillips, Phys. Rev. D **44**, 1987 (1991).

[22] R. M. Barnett, J. F. Gunion, H. E. Haber, I. Hinchliffe, B. Hubbard, and H.-J. Trost, SSC Publication No. SDC-90-00141, 1990 (unpublished); R. M. Godbole and D. P. Roy, Phys. Rev. D **43**, 3640 (1991); L^* Collaboration, Letter of Intent, Publication No. SSCL-SR-1154, 1990; EMPACT Collaboration, Letter of Intent, Publication No. SSCL-SR-1155, 1990.

[23] R. M. Barnett, R. Cruz, J. F. Gunion, and B. Hubbard, University of California, Davis Report No. UCD-92-14, 1992 (unpublished).